Annals of Nuclear Energy 98 (2016) 112–119

Contents lists available at ScienceDirect

Annals of Nuclear Energy

journal homepage: www.elsevier.com/locate/anucene

Preliminary study on the fuel-coolant interaction triggered by thermal effect

Peng Cheng, Tong Lili, Cao Xuewu *

School of Mechanical Engineering, Shanghai Jiao Tong University, Shanghai 200240, China

ARTICLE INFO

Article history:
Received 29 January 2016
Received in revised form 13 July 2016
Accepted 30 July 2016
Available online 6 August 2016

Keywords:
Thermal interaction
Debris
FCI
Severe accident

ABSTRACT

The phenomenon of thermal interaction plays a key role in fuel and coolant interaction (FCI) during NPP's severe accidents, which determines the ratio of heat transferred to mechanical energy. However, the phenomenon is still not well understood due to its transient process and various involved likely mechanisms. In the present study, a new facility for intermediate-scaled FCI experiments has been set up, named ISFCI, mainly concentrating on the influencing factors and thermal interaction mechanism of high melting substances within the confined space. In the first series of tests, 304SS and Fe-Mo have been chosen for the melt materials with superheating temperature ranging from 150 °C to 300 °C. The initial mass of each material has been controlled by 1 kg or 2 kg. By grouping and characterizing the debris, the effect of initial mass, melt properties and melt superheating temperature on thermal interaction has been qualitatively analyzed. In addition, the pressure data recorded from these tests have been used to quantify the influencing analysis. Based on the morphology analyzing method and quantification, two relatively worse conditions that could cause larger and/or longer pressure increase have been identified.

1. Introduction

In severe accident scenarios, the core-melt accident may occur because of lack of sufficient cooling. Without enough coolant supply, the nuclear core starts to degrade from a relatively high position. As the core is partially damaged, core melt may go through downwards into the lower plenum, and even relocate in the lower head of the vessel. If there is a little water remaining in the lower head, maybe a sort of in-vessel vapor explosion can be induced. While if the lower head has already been dried out, the residual melt may continue to melt through the structure, and finally be scattered around the reactor cavity. Once the high temperature melt contacts with the volatile coolant, the fuel-coolant interaction (FCI) can occur, which may result in vapor explosion and seriously damage the reactor cavity or the containment structure. Due to its likely radioactive threats and many uncertain negative effects involved, researchers have drawn much attention to this issue of FCI.

In regards to interpreting the phenomenon of fuel and coolant interaction, a large set of experiments were launched, one of which was large scale tests of corium or stimulant materials. In this group, ALPHA (Yamano et al., 1995; Yamano et al., 1999) researched on the vapor explosion characters, including dynamic pressure history and debris distribution, and pointed out that such involved FCI mechanisms should be figured out. KROTOS (Huhtiniemi and Magallon, 2001; Hohmann et al., 1995; Huhtiniemi et al., 1999) focused on vapor explosion and energy conversion process based on spontaneous trigger or external trigger condition, and firstly presented that the interaction between hot alumina and cold water is much more violent, thus generating a very strong and sharp pressure increase. However, due to lack of FCI mechanism analysis, such new findings could not completely be adopted in mechanistic code for FCI. KAERI carried out the TROI (Song et al., 2002, 2003; Kim et al., 2008) tests, analyzing the specific effect of melt material on vapor explosion, and concluded that ZrO_2 can trigger an even higher vapor explosion. While, if iron was added to the melt, it seemed that the spontaneous vapor explosion was suppressed, but this result still needs to be examined. The other group of experiments was to research on interaction mechanism by small scale tests. For example, SIGMA (Luo et al., 1999) observed the micro-interaction process by high speed camera, and described the mixing region. MISTEE (Park et al., 2009) was highly instrumented by two high speed cameras and an X-ray detector, depicting the premixing and fragmentation process exactly. Besides, SJTU (Lin et al., 2009) systematically analyzed various impact factors on thermal fragmentation mechanisms by SSFT

* Corresponding author.
E-mail address: caoxuewu@sjtu.edu.cn (X. Cao).

http://dx.doi.org/10.1016/j.anucene.2016.07.033
0306-4549/

facility and a typical thermal fragmentation partition map was drawn.

Recently, based on the contribution of OECD (OECD/NEA, 2007), it was recognized that the level of loads would not challenge the integrity of the reactor vessel. However, the problem is that the ex-vessel FCI would probably cause the damage of reactor cavity, affecting the integrity of the containment building. In addition, plenty of FCI codes have been adopted in order to obtain better estimations. People still can't select the best result from those predictions obtained from the codes so far, which makes the potential damage unpredictable. Therefore, further research on the thermal interaction of coolant and melt must be carried out aiming at getting better interpretations of this issue.

SJTU has set up an intermediate-scaled experimental facility named 'ISFCI' to carry out the thermal interaction analysis using stimulant materials. The objective of the ISFCI is to study the mechanisms behind the thermal interaction and develops a new mechanistic model for this process, based on the new experimental findings. In this paper, the first series of test results are presented, in which the debris characteristics under different initial conditions will be firstly described, followed by FCI mechanisms behind. Finally, the corresponding pressures generated from each trial will be qualified and quantified so as to support the analysis of the impact factors.

2. Design of the ISFCI facility

In order to investigate the thermal interaction of coolant and melt, a new facility for intermediate-scaled experiments has been built, which can be schematically shown in Fig. 1. The ISFCI facility consists of a furnace in the upper part, a gate valve, a fast valve in the middle part, a graphite drill at the end of one pipe and a pressure vessel which contains a debris collector in the lower head. All the components are closely connected with each other, in case of pressure loss.

2.1. Furnace and melt release equipment

An induction furnace, which is placed on the second floor of the platform, is designed to heat the experimental material to overheating state in a graphite crucible and the design temperature is around 2000 °C. With the help of the infrared thermometer installed in the center of the furnace lid and the PLC module, the heating temperature could be controlled, stored and presented along the way as well. The graphite crucible is a hollow cylinder, about 300 mm in height, 70 mm in inner diameter and 5 mm in thickness, which can contain 3–4 kg simulant melt at most. Besides, some auxiliary systems must be included, such as prevacuum system, which contains a vacuum pump, some valves and pipes. In order to remove the oxygen from the furnace, the vacuum pump should be used twice prior to the experiment. Considering the request for melt release, the furnace must be maintained in a positive pressure. Therefore, when the oxygen content is relatively low, the protective gas (N_2) is supplied from the protective gas inlet and covers the whole heating zone. When the melt reaches a certain temperature, the graphite crucible drops out of the furnace after pneumatically rotating the platform beneath the heating zone, and the crucible will go through the gate valve. The platform is also controlled by the PLC module and the air supply is from an air compressor (0.9 m^3/min, 1.3 MPa).

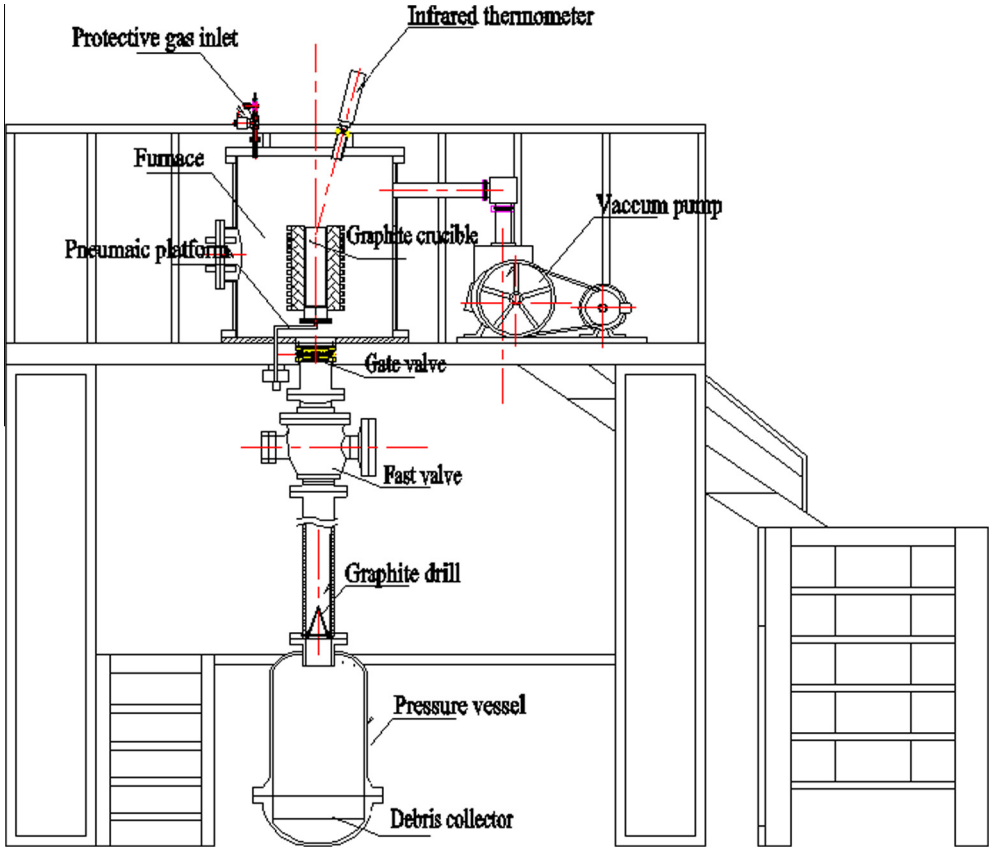

Fig. 1. Schematic diagram of the experimental facility.

2.2. Fast valve and breaching device

Considering the probable strong pressure wave generated from the thermal interaction of coolant and melt, a sort of shutoff device should be installed for the purpose of resisting further devastation. Therefore, a fast valve which is driven by gas expansion is adopted in the test system and the design bearing pressure is around 10 MPa. After the crucible departs from the furnace, it will pass through the fast valve next, and the valve will be completely closed in 0.75 s. It relates to a really quick motion that only electric signal transmission can operate. Therefore, a delay time is added to the release signal, constituting the fast valve control signal. However, it really needs many pretests to determine the delay time in order to make sure that whether the crucible totally passes the valve. Then, the crucible will come to the end of the pressure pipe, where a graphite drill is placed nearby. The graphite drill is a hollow cone, about 129 mm in height, 68 mm in inner diameter, and 98 mm in outer diameter, as shown in Fig. 2. By violent crashing, the melt will come out of the crucible through the breaches and flow away from the 3 circular holes with the diameter of 40 mm on the side wall.

2.3. Pressure vessel and instrumentation

After the melt is away from the pressure pipe, it will directly come to the pressure vessel and contact with the water inside. The pressure vessel is in cylindrical shape, 600 mm in inner diameter and 1350 mm in height. The design pressure of the vessel is determined as 8 MPa, which is much larger than the probable vapor explosion generated from the intermediate-scaled experiments. Due to the temperature rise after the violent interaction, the design temperature of the vessel is determined as 200 °C, which is obtained by multiplying the temperature rise in FARO (Magallon and Hohmann, 1995) by the factor of four. There is a debris collector placed closed to the lower head of the vessel so as to capture those FCI products for post-test analysis. Besides, Table 1 lists the instruments utilized in the experiment and Fig. 3 presents the locations on the side wall.

Thermal couples and pressure transducers are mounted on the sidewall in three different directions, in which part of the instruments are exposed down to the water surface and the rest of them are remained in the atmosphere. In data processing, averaging

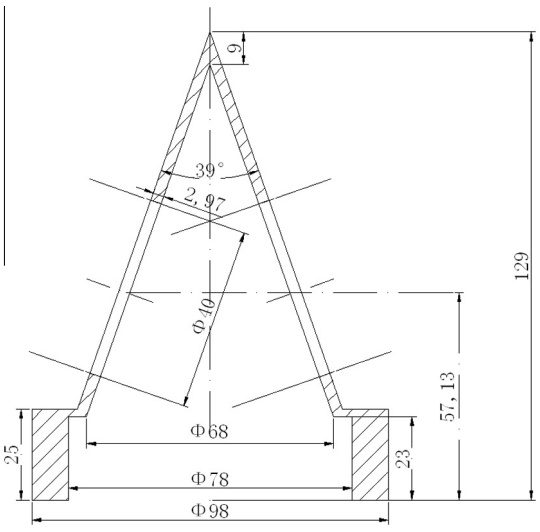

Fig. 2. Structure graphing of the graphite drill.

Table 1
Measurements position and function.

Parameter	Position	Angle	Range	Accuracy	Response time
Lower head	0	–	–	–	–
Coolant temperature T1–T4	1083 mm 933 mm 783 mm 633 mm	0(360°)	0–800 °C	±2.5 °C	1 s
Coolant temperature T5–T8	1083 mm 933 mm 783 mm 633 mm	120°	0–800 °C	±2.5 °C	1 s
Coolant temperature T9–T12	1083 mm 933 mm 783 mm 633 mm	240°	0–800 °C	±2.5 °C	1 s
Transient pressure P1–P4	1083 mm 933 mm 783 mm 633 mm	0(360°)	0–8 MPa	0.1%	5 μs
Transient pressure P5–P8	1083 mm 933 mm 783 mm 633 mm	120°	0–8 MPa	0.1%	5 μs
Transient pressure P9–P12	1083 mm 933 mm 783 mm 633 mm	240°	0–8 MPa	0.1%	5 μs

Fig. 3. Pressure vessel and measuring instrument.

method is adopted to get an equivalent value in each position, which can be expressed as follows.

$$\bar{\phi} = \frac{\phi_{0^\circ} + \phi_{120^\circ} + \phi_{240^\circ}}{3} \quad (1)$$

where the coolant temperature and transient pressure can replace the notation Φ, respectively.

3. First series of test results for Fe-Mo and 304SS

Different combination of temperatures of the melt and coolant has significant effects on the thermal interaction, and the initial

mass, material effect are another key factors, as reported by Lin et al. (2009). Consequently, preliminary test conditions were determined as shown in Table 2.

As mentioned by Peng et al. (2015), the thermal interaction of coolant and melt contains melt jet breakup, premixing, triggering, melt droplet fragmentation, propagation and consequently, steam explosion. Jet breakup is the initial phase of melt and coolant interaction, which can be described as a process that continuous melt jets turn into dispersions. During the premixing phase, the larger dispersions turn into some smaller drops within the millimeter's range. At last, the fragmentation of smaller drops would be induced by some thermal or hydrodynamic forces, such as unstable film boiling effect, surface solidification effect and so on. If such local fragmentation triggers propagation, and then expansion, a real steam explosion would occur.

Based on the debris characteristics, the test products can be classified into two broad classes, including sheet debris and spherical particles. The characteristic scale of sheet debris is generally centimeter scale, whereas the spherical particles can be categorized into two groups based on different equivalent sizes In addition, the peak pressure and duration time in thermal interaction can be used to analyze the effect of initial mass, melt properties and melt superheating temperature, corresponding to the debris analysis.

3.1. The effect of initial mass

In the first series of the tests for initial mass analysis, 1 kg and 2 kg are selected to be the initial mass, so as to research on the effect of initial mass on thermal interaction. Due to the melt retention occurred from the breakup of the graphite crucible to the outflow of the melt, the debris mass from the debris catcher is about 640.26 g and 1718.97 g, respectively.

Compared to the two photos from Fig. 4, it can be seen that part of the products are in regular spherical shape and the rest are sheet debris attached by a large quantity of tiny spherical particles with their ranges from micrometer to centimeter.

From another point of view, debris size distribution can be treated as a piece of direct evidence to judge whether the thermal interaction is violent or not. Therefore, a sieve and a balance are used for post-test classification and statistics, and the result is shown in Fig. 5. Due to the minimum mesh size is around 500 μm (measure limit), the minimum size of the debris is a little larger than 500 μm. All the debris that was collected is categorized into four classes, where the centimeter-scaled debris can be treated as the jet breakup products. As mentioned above, millimeter-scaled debris can be treated as the premixing products. As to those with their size ranging from 500 μm to 1 mm, they can be treated as the fragmentation products, due to some thermal or hydrodynamic forces. The actual mass fraction of premixing products and fragmentation products can be much larger than the present ones, because plenty of debris was attached by tiny particles.

It can be clearly seen from Fig. 5 that the mass fraction of jet breakup products increases with the increase of the initial mass, while the fragmentation products are reduced. It can be explained from the fact that under a certain configuration and test condition, as the initial mass is increased; many jet breakup products are formed by hydrodynamic force or heat transfer. Due to the strong evaporation from the interface, an even thicker and more stable vapor film is formed, thus resisting the direct contact between coolant and melt. Moreover, the premixing process is getting worse, and the fragmentation triggered by unstable film boiling cannot take place. However, there was still large number of tiny particles present in the debris catcher which needs to be paid much attention. Based on the superficial and sectional views of the debris shown in Fig. 6, it can be seen that many hollows and breaches occur on the surface of the products and also cavities remain inside after cutting off the big sheet debris. These characteristics can be attributed to the solidification effect (Cao et al., 2002). When the melt is exposed to coolant, solidification begins on its surface and the molten material is encased in a thin shell. Due to the temperature distribution in the solid shell, the deformation induced in the solid shell tends to compress the inner liquid region, thus strengthening the Taylor instability. At some time, the grown molten metal spikes are broken by turbulent flow and mix with coolant, thus emptying the solid shell. Finally, the 'broken' spikes may be cooled down after departure or prior to departure, thus being attached to the molten jet.

Besides, some unique results can be drawn based on the pressure histories' comparison, as shown in Fig. 7. The peak pressures obtained in Case2 are about 61.654 kPa, 69.442 kPa and 67.295 kPa (from top to bottom) under water, whereas in Case1, they're about 22.664 kPa, 26.442 kPa and 23.305 kPa at the same locations. Obviously, the pressure is becoming larger as the increase of the initial mass. Based on the above analysis of debris size distribution, it can be inferred that the pressure increase is mainly generated from the steam generation by water boiling during the jet breakup phase. However, the reduced mass fraction of premixing products and fragmentation products limits the heat transfer, thus the pressure value is only 2–3 times larger than that in Case1.

Table 2
Design of test conditions.

Case	Material	Melt temperature	Coolant temperature	Initial melt mass	Water level
1	304SS	1600 °C	Ambient temperature	1 kg	~1.008 m
2	304SS	1600 °C	Ambient temperature	2 kg	~1.008 m
3	Fe-Mo	1750 °C	Ambient temperature	1 kg	~1.008 m
4	304SS	1750 °C	Ambient temperature	1 kg	~1.008 m

3.2. The effect of melt properties

In the present study, 304SS and Fe-Mo are selected to be the molten materials with significant difference in density and heat capacity. The main parameters are shown in Table 3. Also, based on the debris collection, the debris mass in Case3 is about 898.80 g. Compared with the two groups of debris, as shown in Fig. 8, it can be seen that there are numerous 'sheet-like' debris. By roughly estimating the heat transfer process from spilling out to landing based on lumped parameter method, the expression can be written as follows,

$$T_m = T_a + (T_{m,ini} - T_a)e^{\left[-\frac{4h}{D\rho_m C_{pm}}\tau\right]} \quad (1)$$

where T_m is the melt temperature, T_a is the ambient temperature, $T_{m,ini}$ is the initial melt temperature, h is the heat transfer coefficient, D is the melt jet diameter, ρ_m is the melt density, C_{pm} is the melt heat capacity.

It can be found that for the Case1, the temperature drop is less than 1 °C in the air, and the final temperature is around 1464 °C, which is a little higher than its melting point. Nevertheless, the temperature drop for Fe-Mo is less than 0.08 °C, and the final temperature is higher than 1700 °C. Therefore, the underlying reason behind the formation of sheet-like products is that the melt still gets a certain degree of superheating when it touches down on the debris collector. It continues to spread out on the collector surface and solidify afterwards. In addition, the heat capacity of Fe-Mo is larger than 304SS's, causing higher superheating temperature, and the density of Fe-Mo is also larger than 304SS's, leading to

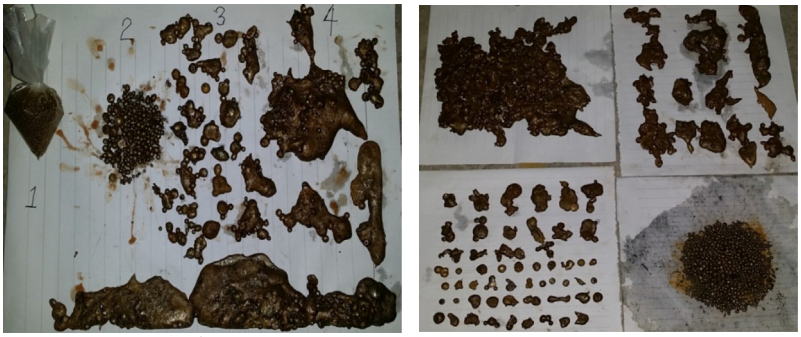

Fig. 4. Debris characteristics.

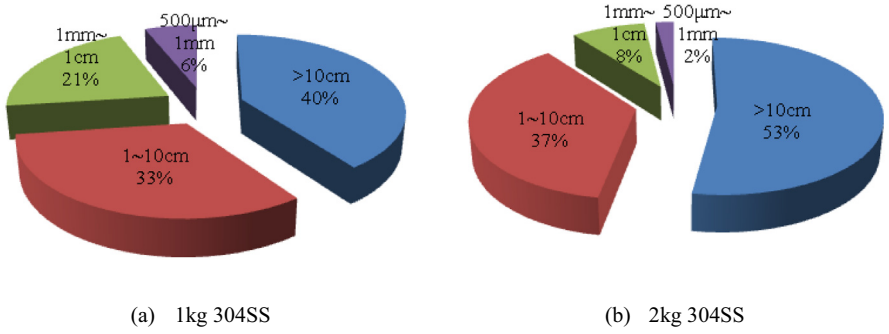

Fig. 5. The mass distribution in terms of debris size.

Fig. 6. Superficial and sectional views of the debris for 304SS with the initial mass of 2 kg.

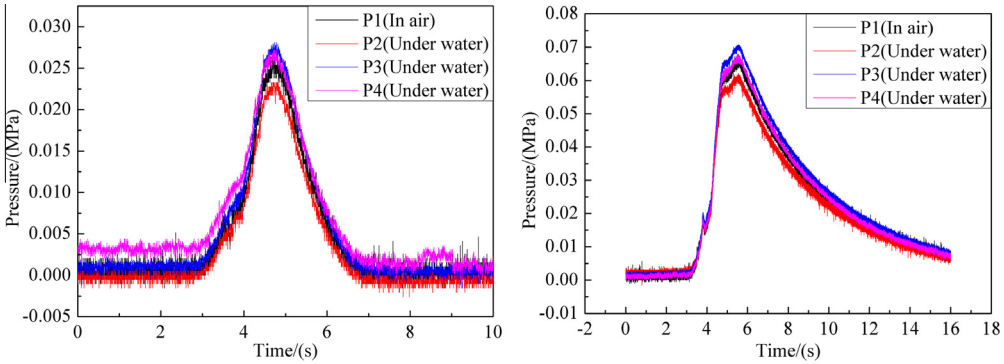

Fig. 7. Pressure histories during thermal interaction (Left: Case1 & Right: Case2).

sustain smaller heat exchange areas for the same total mass. Hence, it's concluded from the fact that Fe-Mo melt forms a multitude of sheet shaped premixing products as soon as it contacts with the collector.

It can be seen from the Figs. 8 and 9 that the mass fraction of Fe-Mo's premixing and fragmentation products is almost around 31%, which is higher than 304SS's. This result suggests that Fe-Mo melt triggers a more violent thermal interaction under the same condi-

Table 3
Thermophysical properties of the melt.

Material	Density kg/m^3	Melting point* °C	Heat capacity J/(kg·K)	Heat conductivity W/(m·K)	Dynamic viscosity mPa·s	Surface tension mN/m
304SS	6780	~1450	800	30	6.35046	1790
Fe-Mo	9000	~1600	2386.5	≪30	>6.44	~2040

* The melting point varies depending largely on different impurity contents (or molybdenum content).

(a) Case1 304SS/1600℃/1kg/26.5℃ (b) Case3 Fe-Mo/1750℃/1kg/28.5℃

Fig. 8. Debris characteristics for 304SS and Fe-Mo.

tion. As mentioned above, with the increasing of the melt surface, the heat exchange areas will also be enlarged later on. Meanwhile, Fe-Mo can sustain even higher superheating temperature all along. It can be speculated that the premixing zone in Case3 is larger than in Case1, thus inducing a much more complete premixing. As to the fragmentation products involved, it seems that the fragmentation process is slightly influenced by the effect of melt properties, which is much different from those discovered by many researchers before, such as the conclusions from KROTOS tests (Huhtiniemi et al., 1997; Hohmann et al., 1995), SIGMA tests (Luo et al., 1999), SSFT test (Lin et al., 2009), BNL test (Ciccarelli and Frost, 1994), MISTEE tests (Park et al., 2009) and so on. Both small-scaled and large-scaled experiments are used to prove that the effect of melt properties has significant influence on fragmentation process. However, what is worth to mention is that the steam explosion occurred in their experiments, which means that the better-premixing must be built, corresponding to the conclusions from Cho (Corradini et al., 1989), who proved that the premixing is the most important and favourable phase to fragmentation, and then steam explosion. Therefore, a probable explanation that the worse-premixing resulted in poor fragmentation is given. Then, how to distinguish between the better-premixing and worse-premixing in reality? A definition has been proposed, which is called "critical premixing limit". This definition refers to that there may be a critical line of premixing ratio for each system (certain geometrical configuration and physical condition). Only if the local premixing ratio is beyond this barrier, the fragmentation process would be severely influenced by the melt properties and if the premixing ratio is below this critical line, the melt properties would have little effect on the fragmentation process. However, it seems that the present cases belong to the latter condition. This proposal will be further studied in the next series of experiments.

Similarly, some parallel results can be obtained based on the pressure histories, as shown in Fig. 10. The peak pressures obtained in Case3 are about 104.263 kPa, 121.067 kPa and 116.484 kPa (from top to bottom) under water, whereas in Case1, they're about 22.664 kPa, 26.442 kPa and 23.305 kPa at the same locations. The large difference in pressures reveals that the thermal interaction taking place in Case3 is more violent than Case1, and thus results in much finer debris. Based on the above analysis of debris size distribution, it can be inferred that the pressure increase is most likely to be generated from the premixing phase. By liberal estimates, as the mass fraction of premixing increases 4%, the outcome will be that the pressure increase is five to six times higher than original. Therefore, based on the pressure histories during thermal interaction, the influence of melt properties on thermal interaction cannot be ignored. In addition, the longer duration time can also be viewed as a significant characteristic for the thermal interaction of coolant and melt. Due to the large heat capacity and density, the thermal inertia of Fe-Mo is relatively large, thus maintaining the pressure transmitting process for several seconds. From the above, a relatively worse condition determined from the present study is that a much stronger pressure increase would be induced and maintains a long transmission time, when the melt gets a larger density and heat capacity.

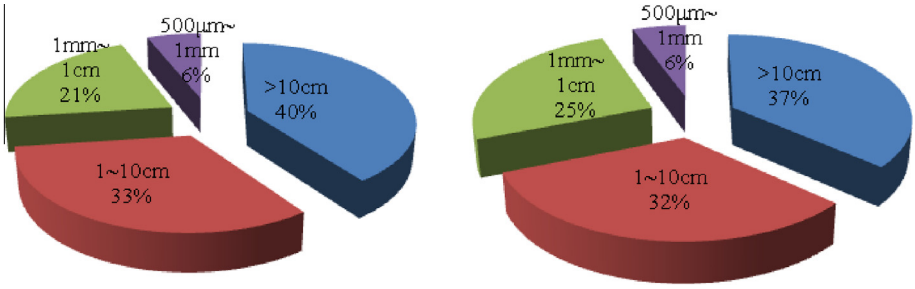

Fig. 9. The mass distribution in terms of debris size.

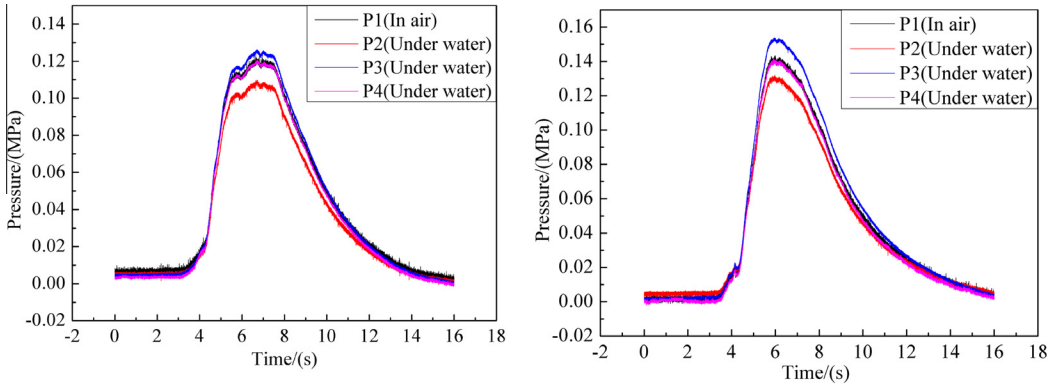

Fig. 10. Pressure histories during thermal interaction (Left: Case3 & Right: Case4).

3.3. The effect of melt superheating temperature

In Case4, the debris mass is about 742.14 g and the debris collected from Case4 are shown in Fig. 11, which demonstrates that almost 14% of total mass are for spherical fine debris or tiny particles with its size in micrometer range. This ratio illustrates that the fragmentation taking place in Case4 is more violent than that in Case1. In other words, the size of debris varies largely depending upon the melt superheating temperature. Based on the concept of critical premixing limit, as mentioned above, it seems that the melt superheating effect can tremendously strengthen the premixing phase, thus making the melt much more premixed. Moreover, as some local premixed mass fraction may exceed the critical limit, the local fragmentation will become stronger. Therefore, the melt superheating effect can be regarded as one of the main factors to stimulate the premixing and fragmentation process. Similarly, the fragmentation can be explained by the surface solidification mechanism, too. With the increase of the penetration length, a solid shell covers the molten material. Due to the temperature distribution in the solid shell, the deformation induced in the solid shell tends to compress the inner liquid part, and thus leads to fragmentation. The model has been proposed by Cao et al. (2002), which can be expressed as formula (2) and formula (3).

$$\Gamma_{ss} = 2.1 \times 10^{-2} Bi^{0.1} \left(\frac{\alpha_t (T_m - T_c) E}{R^2 \rho_m} \right)^{0.5} \tag{2}$$

$$d_{frag} = \left(\frac{2 d^3 \sigma_t}{1.54 \times 10^{-2} Bi^{0.12} \alpha_t E (T_m - T_c)} \right)^{0.25} \tag{3}$$

where Γ_{ss} is the fragmentation rate, defined as normalized fragmented mass of a droplet per second, T_m is the melt temperature, T_c is the coolant temperature, d_{frag} is the fragment size. Based on the formulas (2) and (3), it can be seen there is a positive correlation between the fragmentation rate and the term of $(T_m - T_c)^{0.5}$ and a negative correlation between the size of the fragments and the term of $(T_m - T_c)^{0.25}$. Therefore, it's clear to confirm that the mass ratio of fragmentation products in Case4 is even higher than in Case1 and the size of fragments decreases with the increase of the melt superheating temperature as well.

In addition, according to the pressure histories during thermal interaction as shown in Fig. 10, several similar conclusions can be drawn. The peak pressures obtained in Case4 are about 130.944 kPa, 153.887 kPa and 140.974 kPa (from top to bottom) under water, whereas in Case1, they're about 22.664 kPa, 26.442 kPa and 23.305 kPa at the same locations. In the first place, it can generate a much higher pressure under the condition of 300 K in melt superheating temperature, which has been verified by Cao's correlation (Cao et al., 2002). Besides, based on the above analysis of debris size distribution, it can be seen that the pressure increase is mostly generated from the premixing and fragmentation phase. Also by liberal estimates, as the mass fraction of premixing increases 6%, the pressure increase will be five to seven times higher than original, which agrees well with the conclusion before. Hence, the peak pressure increases with the melt superheating temperature, if other initial conditions are the same. In the second place, the duration time for pressure transition can be prolonged with the increase of the melt superheating temperature. It seems obvious that the duration time for Case4 is around 12.8 s, whereas it is 4 s for Case1 at most. The reason behind can be described as the large quantity of thermal energy is in store for evaporation due to the higher superheating temperature in Case4, and then the strong evaporation tries to remedy the pressure drop, thus prolonging the duration time of peak pressure. From the above, another relatively worse condition determined from the present study is that a much stronger pressure increase would be

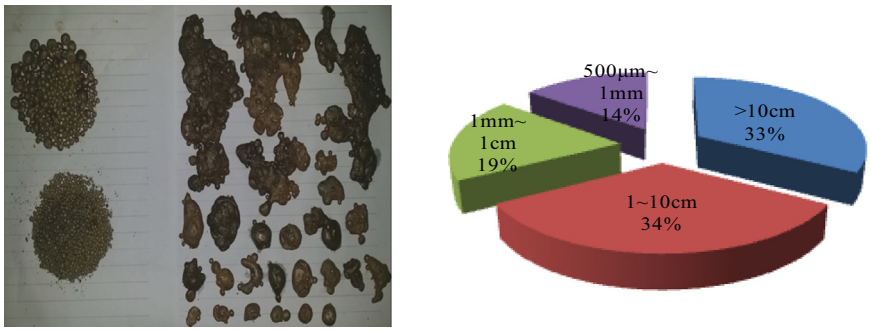

Fig. 11. Debris characteristics for 304SS (1750 °C/1 kg/29.5 °C).

induced and maintains a long transmission time, when the melt gets a higher superheating temperature.

4. Conclusions

In this paper, the test facility and conditions for thermal interaction of coolant and melt have been introduced at first. Then, four groups of experimental results have been analyzed based on the effects of initial mass, melt properties and melt superheating temperature. With the help of the morphology method and the pressure recorded by pressure transducers, the main conclusions can be drawn, as follows.

(1) Compared with Case1 and Case2, the mass fraction of jet breakup products increases with the increase of the initial mass, while the fragmentation products are reduced. It can be inferred from the fact that under a certain configuration and test condition, whether the premixing zone is large or not has a significant effect on the thermal interaction strength.
(2) Density and heat capacity of the melt are the influencing factors to affect the premixing, and a relatively worse condition determined from the present study is that a much stronger pressure increase would be induced and maintains a long time, when the melt gets a larger density and heat capacity.
(3) The melt superheating effect can significantly strengthen the mass fraction of premixing products and thermal fragmentation ratio. Similarly, another relatively worse condition determined from the present study is that a much stronger pressure increase would be induced and maintains a long time, when the melt gets a higher superheating temperature.

All in all, there were only mild interactions happening in the first series of tests, and it can be inferred that it's the 'stable system', such as inert melt properties or lower water depth, that may suppress the vapor explosions induced by the interaction of coolant and melt. Therefore, some tests based on higher water depth or different melt mass in different superheating temperature should be performed for the purpose of better interpreting this kind of issue.

Acknowledgments

This work was supported by National Natural Science Foundation of China (No. 11375116) and National Science and Technology Major Project of the Ministry of Science and Technology of China (2013ZX06004008-006).

References

Cao, X.W. et al., 2002. A thermal fragmentation model induced by surface solidification. J. Nucl. Sci. Technol. 39 (6), 628–636.
Ciccarelli, G., Frost, D.L., 1994. Fragmentation mechanisms based on single drop steam explosion experiments using flash X-ray radiography. Nucl. Eng. Des. 146, 109–132.
Corradini, M.L. et al., 1989. Vapor explosion in light water reactor: a review of theory and modeling. Prog. Nucl. Energy 22 (1), 1–177.
Hohmann, H. et al., 1995. FCI experiments in the aluminum oxide/water system. Nucl. Eng. Des. 155, 391–403.
Huhtiniemi, I., Magallon, D., 2001. Insight into steam explosions with corium melts in KROTOS. Nucl. Eng. Des. 204, 391–400.
Huhtiniemi, I. et al., 1997. FCI experiments in the corium/water system. Nucl. Eng. Des. 177, 339–349.
Huhtiniemi, I. et al., 1999. Results of recent KROTOS FCI tests: alumina versus corium melts. Nucl. Eng. Des. 189, 379–389.
Kim, J.H. et al., 2008. Steam explosion experiments using partially oxidized corium. Mech. Sci. Technol. 22, 2245–2253.
Lin, Q. et al., 2009. Thermal fragmentation process of melt droplet. At. Energy Sci. Technol. 43 (7), 604–608.
Lin, Q. et al., 2009. Experiment on fragmentation of melt drop interacted with water. Nucl. Power Eng. 30 (1), 31–35.
Luo, R. et al., 1999. Experimental simulation of microinteractions in large scale explosions. Nucl. Eng. Des. 189, 163–178.
Magallon, D., Hohmann, H., 1995. High pressure corium melt quenching tests in FARO. Nucl. Eng. Des. 155, 253–270.
OECD/NEA, 2007. Research Program on Fuel-coolant Interaction-SERENA Steam Explosion Resolution for Nuclear Applications. Final Report. NEA/CSNI/R (2007) 11.
Park, H.S. et al., 2009. Dynamics and preconditioning in a single-droplet vapor explosion. Nucl. Technol. 167, 223–234.
Peng, C. et al., 2015. A hydrodynamic fragmentation model based on boundary layer stripping. Ann. Nucl. Energy 80, 95–100.
Song, J.H. et al., 2002. Experiments on the interactions of molten ZrO_2 with water using TROI facility. Nucl. Eng. Des. 213, 97–110.
Song, J.H. et al., 2003. Fuel coolant interaction experiments in TROI using a UO_2/ZrO_2 mixture. Nucl. Eng. Des. 222, 1–15.
Yamano, N. et al., 1995. Phenomenological studies on melt-coolant interactions in the ALPHA program. Nucl. Eng. Des. 155, 369–389.
Yamano, N. et al., 1999. Study on premixing phase of steam explosion at JAERI [J]. Nucl. Eng. Des. 1999 (189), 205–221.